Hindawi
Shock and Vibration
Volume 2021, Article ID 4981507, 12 pages
https://doi.org/10.1155/2021/4981507

*Research Article*

# Numerical and Experimental Approach for Failure Analysis of Soil Subjected to Surface Explosion Loading

**Iau-Teh Wang**

*Department of Civil Engineering, R.O.C Military Academy, Kaohsiung 830, Taiwan*

Correspondence should be addressed to Iau-Teh Wang; itwangroc@gmail.com

Received 27 April 2021; Accepted 8 July 2021; Published 16 July 2021

Academic Editor: Nan Jiang



Controlling the hazards to facilities caused by detonation waves is a high priority in engineering design. To protect an underground facility, soil can reduce the destructive effects of detonation waves. Soil dynamic characteristics and the area of the destructive zone are affected by shock wave energy. The material at ground zero is impacted by high-intensity stress and forms a crater. To ensure the safety of the facility, the protective soil layers must be sufficiently thick. Therefore, the purpose of this study was to analyze the destructive effects that caused the deformation and destruction of an external protective soil layer. The results of the explosion experiments and the numerical simulation analysis were compared to explore the dynamic characteristics of the soil affected by the shock wave and the crater effects of on-ground explosions. The analysis model adopted an 8-node hexahedral element to create a three-dimensional solid structure model of the fluid-solid interaction. The material failure analysis demonstrated that the detonation wave destabilized the interior of the soil body, and the nearby high-intensity stress was the key factor for material failure. The results can serve as a reference for the design of soil-covering layers that provide explosion hazard control.

## 1. Introduction

Structural protection engineering is the essential design principle for vital industries and national defense infrastructure. Burster layers can be used to reduce the damage caused by blast effects to protect essential engineering facilities. Before designing military and industrial pipelines, it is necessary to calculate the area and extent of the explosion destruction effect to calculate the thickness of the protective layer. The detonation wave is transmitted outward through the medium; the generated stress wave induces particle vibration in the medium and affects the internal stability of the material [1–4]. The explosion shock wave compresses the ground and pushes soil, forming a crater. The extent of destruction and the affected range are determined by the energy of the shock wave and the material characteristics of the transmission medium [5]. Schenker et al. [6] investigated the explosion pressure generated by indoor explosions. Their results showed that the relative error between the shock pressure obtained from experiments and numerical analysis was 15%, and the relative error of the impulse was approximately 9%. Wang and Lu [7] explored the shock wave energy generated by an explosion. Their results indicated that the energy released near the explosion source was high and the effect of the compression wave on the soil was relatively high. Crandle [8] analyzed the transmission of detonation waves and the factors that affected the vibration intensity. The results indicated that the transmission process of detonation wave induced particle vibration and caused different degrees of destruction to the medium. Koga and Matsuo [9] studied an explosion caused by burying explosives in soil. Part of the energy of the detonation wave was converted into seismic waves in the transmission process; those seismic waves induced particle vibration. Wang et al. [10] studied the seismic waves of a low-altitude explosion that were primarily generated by a shock wave in the air; the seismic waves were transmitted in the form of shock waves and then converted into elastic seismic waves, inducing particle vibration on the surface. Soil compression waves were generated by the ground compression induced by the air shock wave generated during an on-ground explosion. The compression wave eventually transformed into an elastic

seismic wave. Wang [11] applied a numerical analysis model of explosion pressure verification to an explosion experiment to prove that the LS-DYNA finite element program could effectively analyze the transmission behavior of a detonation wave during an on-ground explosion.

Soil strength impedes soil failure or sliding along any plane in the soil body. If soil has strength, then that soil maintains a certain shape. Soil strength provides stability in ultimate stress states, including stresses from soil weight or external loading. The principal reason for material failure is that the combination of normal and shear stresses reaches a critical state. If the shear stress exceeds the ultimate strength, the soil equilibrium state is upset and causes soil failure [12]. The process of soil loading and unloading during detonation wave transmission is an irreversible stress-strain relationship. When the detonation wave reaches the ground, the pressure increases rapidly and passes down to the interior of the soil. This state is referred to as overstress. The transmission of overstress in soil is a complicated topic. Under explosion dynamics, the yield criterion of a soil body can be defined as the amount of excessive deformation. On-ground explosions are converted into mechanical energy and thermal energy and cause medium deformation and crater [1].

According to the impact caused by a shock wave, compression, fracture, and vibration zones can be identified outside the explosion center. An on-ground explosion induces high temperature, high pressure, and detonation waves on the soil and causes soil compression, deformation, and the throwing phenomenon, resulting in crater [13]. Ambrosini and Luccioni [14] analyzed the energy released by the explosion of a unit volume of explosives through the crater effect. Bazant and Belytschko [15] analyzed the transmission of transient dynamic waves in strain-softening media and verified the phenomenon of localized strain softening in materials. The phenomenon of strain softening causes the stress to decrease with the increase in strain. Clough and Woodward [16] applied deformation analysis to geological engineering research; they analyzed the stress, strain, deformation, and displacement of an object under the effects of its weight or external forces. Based on the constitutive law, the equilibrium equation, and the deformation geometry law of continuum mechanics, the deformation analysis method was used to analyze the stresses and strains of different material compositions and the deformation geometries of different combinations of strain and displacement. A previously published study considered the characteristics of heterogeneous materials and explored material composition including linear elastic and nonlinear stress-strain relationships. The same study also investigated plastic behavior models to explore material behaviors induced by external forces such as stress, strain, deformation, and displacement.

On the ground, the explosion shock wave affects the stability of the material and causes different degrees of crater destruction on target objects [17]. This study analyzed the extent of destruction and impact of on-ground explosions on protective soil layers. In the context of the yield strength and failure criteria of the material, this study analyzed the destruction radius, diameter, and destruction depth of craters to evaluate the extent of destruction caused by the crater effect of explosions.

The shock analysis was completed within a few milliseconds, and the discussion of destructive effects was focused on the dynamic soil response and the level of damage by shock waves. Given the spatial limitations of the experimental site and legal restrictions on the amount of explosive use, a large-scale explosion experiment is not feasible. According to the nature of the research questions, to enhance the accuracy of numerical analysis, this study employed a fluid-solid coupling finite element approach in conjunction with an explosion experiment that resulted in craters was used to verify the accuracy of the element erosion estimation. Exploring the transmission of shock waves in the soil, this study determined the optimal benefits of the parameters of soil element failure caused by contact explosions to establish the foundation of a dynamic numerical model.

## 2. Experimental Configuration

This study adopted on-site experiments and numerical simulation analyses to explore the deformation and destruction effects of explosions. The amount of trinitrotoluene (TNT) explosives in each of the three crater explosion experiments was the same. The effects of explosions on the crater effect of the soil were tested with explosives positioned upright on the ground.

Figure 1 shows the configuration of the experiment site for measuring the ground acceleration and apparent crater of explosion. This study used explosions to obtain experimental coefficients of ground acceleration to verify the accuracy of the numerical analysis model. In the on-ground explosion testing, 226.796 g (0.5 lb) TNT explosive was placed upright on the ground. Three-axis accelerometers were arranged at 350 and 500 cm from the explosion center to quantitatively analyze the ground accelerations on $X$, $Y$, and $Z$ directions. The accelerometers measured the ground accelerations of explosion vibration. The signals went through an oscilloscope and to a signal conditioner for data transmission and storage. The experimental instrument included three-axis accelerometers, power supply systems, oscilloscopes, signal conditioners, and data acquisition systems.

## 3. Numerical Analysis Approach

The crater effect of explosions is highly nonlinear. Most related studies have focused on analyzing the characteristics of transmission medium failure caused by the shock wave. Explosion experiments are costly, the experimental sites are restricted, and the experiments can be dangerous. Using computer-aided engineering analysis can avoid the hazards of the explosion process. This study verified the results of explosion experiments by using numerical simulation. Numerical analysis based on the finite element method was conducted using hydrodynamic code in LS-DYNA. The Multi-Material Arbitrary Lagrangian–Eulerian (MMALE)

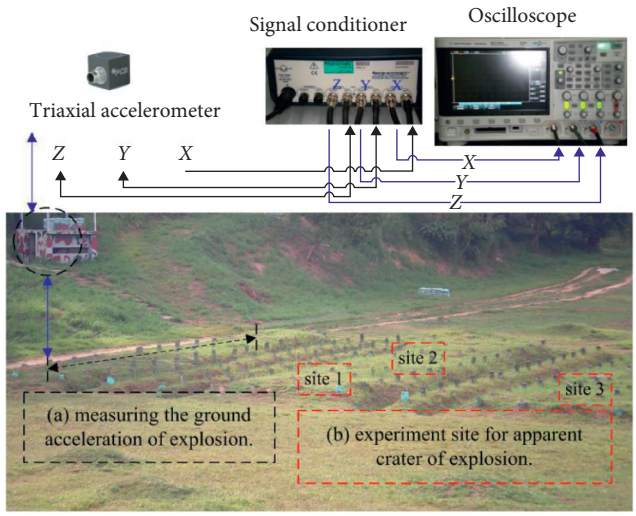


FIGURE 1: Configuration of the explosives in the field experiment. (a) For the ground acceleration measurement. (b) For testing the apparent crater effect of explosions.

algorithm was integrated with the 8-node solid element to establish a three-dimensional (3D) solid structure model of the fluid-solid interaction.

*3.1. Control of Time Stop and Element Type.* The numerical analysis tool for exploring explosion effects must satisfy the coupling between the hydrodynamic state and the solid. The LS-DYNA nonlinear finite element analysis program is based on the mechanics of the continuous medium and employs the explicit time integration method to calculate dynamic mechanical characteristics. Using explicit time integration analysis to investigate the instantaneous dynamics of explosions is conditionally a stable calculation method that requires time step ($\Delta t$) control.

The conditional stability of explicit time integration is affected by the time step. However, when using explicit time integration, the time step must be less than the critical time interval, which is affected by its control factor (TSSFAC) (1). The program automatically divides time ($T$) into $T/\Delta t$ cycles, and the LS-DYNA program manual suggests that the time step control factor should be set in the range 0.1~0.9 and that for the explosion analysis should be lower than 0.67 [18, 19].

$$\Delta t = \text{TSSFAC} \cdot \frac{l_{\text{mesh}}}{C_l}, \tag{1}$$

where $l_{\text{mesh}}$ is the minimum mesh size, and $C_l$ is the wavelength.

The operations of finite element analysis require algorithms and element types that are appropriate for the material characteristics. The numerical calculation of motion in this study used the MMALE algorithm, which adopted 8-node hexahedral elements for analysis. The element is a 3D solid structure model and the shape function is expressed as in (2); the coordinates ($\xi_j$, $\eta_j$, and $\zeta_j$) are associated with different node positions and the values are ±1. Eight nodes were defined in the element; each node had degrees of freedom for translation, velocity, and acceleration in the $X$, $Y$, and $Z$ directions. This element was suitable for explicit dynamic analysis [18, 19].

$$\phi_j = \frac{1}{8}\left(1 + \xi\xi_j\right)\left(1 + \eta\eta_j\right)\left(1 + \zeta\zeta_j\right). \tag{2}$$

The MMALE algorithm exhibits the advantages of the Eulerian and Lagrangian algorithms. The Eulerian algorithm is used to arrange the element meshing to separate the mesh from the analyzed object, overcoming the negative volume caused by the severe mesh distortion. The Lagrangian algorithm is used for the material boundary analysis, which can effectively track the displacement and deformation of structural boundaries. For the dynamic analysis of the fluid-solid interaction, fluid is analyzed using the Eulerian algorithm to fix the nodes of the element mesh in the structure space. Only the material particles flow in the space. The solid is analyzed using the Lagrangian algorithm, and the material particles move with the deformation of the continuum, which is helpful for the deformation analysis of the movement of the fluid-solid interaction [20–22].

*3.2. Element Erosion Criterion.* Soil is a three-phase system composed of solid, liquid, and gas phases. For models of soil composition, yield criterion, stress, and strain analysis, the applicable conditions and material characteristics must be considered and the dynamic response of the pore material induced by the explosion force must be effectively analyzed. The Krieg yield criterion is based on isotropic plasticity theory, and the yield function is presented as in (3) The yield planes, $J_2$ and $\sigma_y$, are presented as in (4) and (5), where $a_0 = c^2$, $a_1 = 2c \tan \phi$, and $a_2 = \tan^2 \phi$. Before the material yields, a linear elastic relationship exists between the stress and strain. The relationship between the stress and strain of the plastic state conforms to the rule of plastic flow, and the material failure is determined according to the shear stress. Based on the strain after yielding, the stress zone of pore materials (e.g. soil, rock, concrete, foam, and honeycomb materials) can be divided into hydrostatic pressure and shear stress zones, which can be used to analyze the effect of pressure on the compaction and destruction of the material. It can be applied to numerical analysis programs such as LS-DYNA, ANSYS, and MSC/DYTRAN.

$$\phi_{\text{yield}} = J_2 - \left(a_0 + a_1 p + a_2 p^2\right), \tag{3}$$

$$J_2 = \frac{1}{3}\sigma_y^2, \tag{4}$$

$$\sigma_y = \left[3\left(a_0 + a_1 p + a_2 p^2\right)\right]^{1/2}, \tag{5}$$

where $J_2$ is the second invariant of the deviatoric stress, $p$ is the pressure, $a_0, a_1, a_2$ are the shear force yield plane coefficients, and $\sigma_y$ is the axial yield stress.

The shear stress of the octahedral stresses is a function of $J_2$. The normal stress of the octahedral stresses is equivalent to the average value of the principal stress as in (6). The relationship between the maximum shear stress is given in

equation (7), and the second invariant of the deviatoric stress is presented as in (8). For the pure shear stress, $\sigma_1 = \tau > 0, \sigma_2 = 0, \sigma_3 = -\tau$, and the shear stress ($\tau$) is defined as $\sqrt{J_2}$, $\tau_{oct} = \sqrt{J_2} = \tau$.

$$\sigma_{oct} = \frac{1}{3}(\sigma_1 + \sigma_2 + \sigma_3), \tag{6}$$

$$\tau_{oct} = \frac{\sqrt{2}}{3}\sqrt{\sigma_1^2 + \sigma_2^2 + \sigma_3^2 - \sigma_1\sigma_2 - \sigma_1\sigma_3 - \sigma_2\sigma_3}, \tag{7}$$

$$\tau_{oct} = \frac{\sqrt{2}}{3}J_2, \tag{8}$$

where $\sigma_{oct}$ is the octahedral normal stress, $\tau_{oct}$ is the octahedral shear stress, and $\sigma_1, \sigma_2, \sigma_3$ are the maximum principal stress, middle principal stress, and minimum principal stress.

The soil constitutive law used in this study must consider the stress and strain behaviors of the pore material caused by pressure. Schwer [23] proposed that the shear failure criterion of the soil/rock model in LS-DYNA reveals a relationship between the mean stress and failure strength. The Krieg yield criterion can calculate the dynamic response in the soil and is also suitable for the analysis of 3D models. Therefore, this study used the Krieg yield criterion as its constitutive law for analyzing the characteristics of soil.

The overstress transmitted by a detonation wave in soil is an irreversible stress-strain relationship. The energy transmission and conversion process of the explosion causes destruction to soil and forms a crater. The finite element erosion algorithm is conducted based on the pressure, stress, and strain of the material. The high strain rate generated by the explosion shock wave affects the internal stress variation of the soil, resulting in strain in the soil. The soil yield criterion can be defined as the amount of excess deformation. LS-DYNA defines element failure and erosion criteria by MAT_ADD_EROSION. The failure element is thus removed from the material model. On the basis of the relationship between stress and strain of material, this study used the failure shear strain as the elemental erosion failure criterion and for soil destruction area analysis. If the material failure criterion $\gamma_1 \geq \gamma_{max}$ is met, the element in the model is deleted, as presented in [19], where $\gamma_1$ is the maximum shear strain, $\gamma_1 = (\varepsilon_1 - \varepsilon_3)/2$, $\varepsilon_1$ is the maximum principal strain, $\varepsilon_3$ is the minimum principal strain, and $\gamma_{max}$ is the shear strain at failure.

*3.3. Nonlinear Dynamic Models.* To verify the numerical model, the 1/4 symmetric numerical analysis model was established according to the experimental conditions of ground acceleration in the experiment. The fluid and the solid meshes were independent from each other. The solid mesh size was twice that of the fluid mesh. The fluid mesh adopted the common point mode and the solid mesh adopted the contact mode. The fluid-solid coupling was established using the mesh overlap method [24]. The size of the mesh was determined based on the minimum width of the TNT explosive. The application of finite element analysis requires consideration of the complexity of an analysis model and the mesh size. To enhance the calculation accuracy, adopt a fluid dynamic analysis program LS-DYNA, finite element analysis software, to conduct the fluid-solid interaction. A TNT free-field explosion simulation is analyzed for mesh size convergence under an explosive load. The analysis results reveal the optimal mesh size is 0.5 times that of the side length of the TNT. The time step control parameter was set to 0.3 [25]. The fluid-solid interaction numerical analysis model of the MMALE algorithm was established through the use of the definition of LS-DYNA CONSTRAINED_LAGRANGE_IN_SOLID and the 3D solid elements. The explosives and air mesh were defined by the Eulerian algorithm, and the soil mesh was defined by the Lagrangian algorithm.

Figure 2 shows a 1/4 symmetry model for numerical simulation analysis of explosion-induced ground acceleration. The dimensions of the air model were $550 \times 500 \times 200$ cm. The density of the TNT explosive was 1.63 g/cm$^3$, the weight was 226.796 g (0.5 lb), and the dimensions of the model were $3.28 \times 3.28 \times 9.3$ cm. The explosive was placed in the center of the model and was on the ground. The dimensions of the soil model were $550 \times 350 \times 200$ cm. The dimensions of the finite element mesh of air, explosives, and soil were $1.64 \times 1.64 \times 3.28$ cm.

Figure 3 shows a 1/4 symmetry model for numerical analysis of crater failure effects. The dimensions of the air model were $120 \times 150 \times 120$ cm. The dimensions of the soil model were $120 \times 120 \times 120$ cm. The cuboidal TNT explosive sample was placed on the ground at the center of the model and the density was 1.63 g/cm$^3$. The amounts of TNT explosive were 113.389 g (0.25 lb), 226.796 g (0.5 lb), and 453.592 g (1.0 lb), which were selected to analyze the crater effect of placing dynamite samples upright on the ground. The dimensions of the 113.389 g, 226.796 g, and 453.592 g TNT models were $1.64 \times 1.64 \times 9.3$ cm, $3.28 \times 3.28 \times 9.3$ cm, and $6.56 \times 6.56 \times 9.3$ cm. The dimensions of the finite element mesh of air, explosive, and soil were 0.82, 0.82, and 1.64 cm, respectively.

*3.4. Material Constitutive Laws.* The internal constitutive law of the material is presented by the relationship between the stress tensor and strain tensor. The equation of state (EOS) describes the relationship between pressure, temperature, density, internal energy, and change in volume after a material has been impacted by external force. The analysis of explosion phenomena must be paired with the corresponding equations of state to satisfy the dynamic response and volume change of the analyzed material after the material has been affected by the explosion force.

Soil from the explosion site was sampled for analyzing the physical and mechanical characteristics, and the Unified Soil Classification System (USCS) was applied for the categorization. According to the results of laboratory analysis, the soil moisture content of the explosion site was 12.8%, density was 2.6 g/cm$^3$, cohesive $c = 8.43$ kg/cm$^2$, and friction angle $\phi = 14°$. The classification symbol was SP-SM, which referred to poorly graded sand with silt.

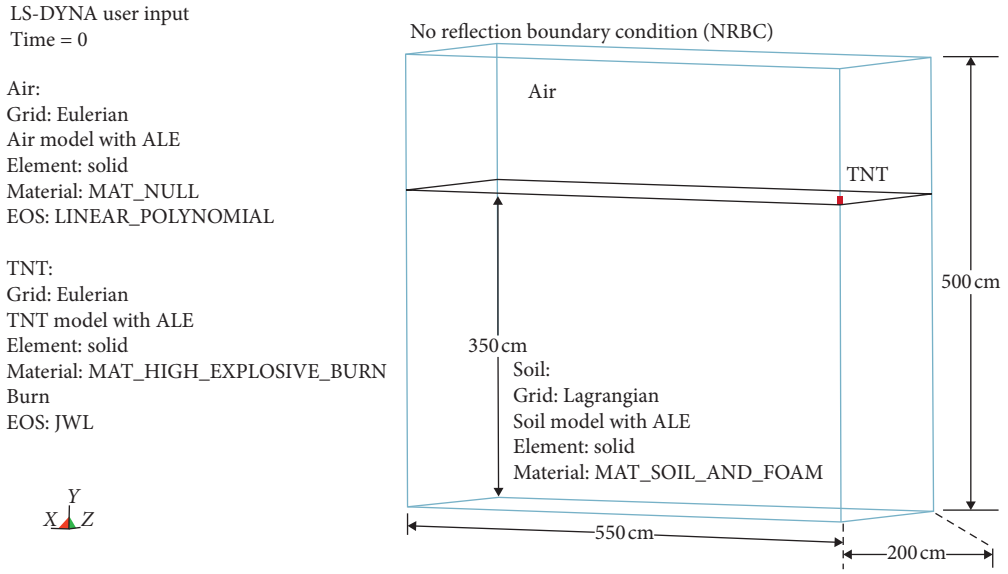


Figure 2: Numerical analysis of the 1/4 symmetry model of the ground acceleration induced by explosion.

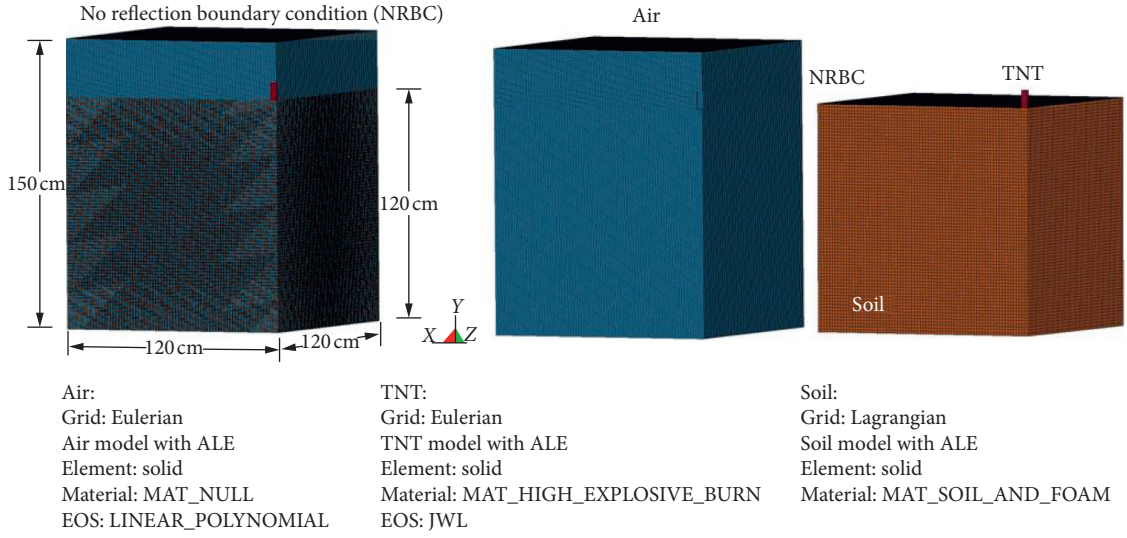


Figure 3: Numerical analysis of the 1/4 symmetry model of the explosion crater effect caused by material failure.

The soil constitutive law must be able to effectively simulate the crushing or compacting behavior of the pore material and the dynamic response after the material has been affected by the explosion. According to the material characteristics, this study selected the MAT_SOIL_AND_FOAM material model to analyze the dynamic response characteristics of the soil. The soil parameters are, respectively, elastic modulus $E = 43.75$ MPa, shear modulus $G = 14.68$ MPa, bulk modulus $K_v = 729$ MPa, and shear-yield surface parameters $a_0 = 7.105 \times 10^{-7}$, $a_1 = 4.198 \times 10^{-8}$, and $a_2 = 6.215 \times 10^{-10}$.

The TNT explosive model used the MAT_HIGH_EXPLOSIVE_BURN material model. Combined with the Jones–Wilkins–Lee (JWL) equation of state analysis in (9), the phenomena of the high speed, high temperature, high pressure, and rapid energy-releasing high explosives were simulated. The parameters are, respectively, $A = 3.712 \times 10^{11}$ Pa, $B = 3.231 \times 10^{9}$ Pa, $R_1 = 4.15$, $R_2 = 0.95$, $\omega = 0.30$, $V = 1.0$, $E_0 = 4.29 \times 10^{6}$ J/kg, initial density is 1630 kg/cm$^3$, and its detonation velocity is 6930 m/s [19, 26, 27].

$$p = A\left(1 - \frac{\omega}{R_1 V}\right)e^{-R_1 V} + B\left(1 - \frac{\omega}{R_2 V}\right)e^{-R_2 V} + \frac{\omega E_0}{V}, \quad (9)$$

where $p$ is the pressure, $V$ is the relative volume, $E_0$ is the initial internal energy per unit reference specific volume, and $A$, $B$, $R_1$, $R_2$, and $\omega$ are the constants representing characteristics of the explosive.

The air model used the MAT_NULL material model and was analyzed using the EOS_LINEAR_POLYNOMIAL in (10). The coefficients in the LINEAR_POLYNOMIAL are

$C_0 = C_1 = C_2 = C_3 = C_6 = 0$ and $C_4 = C_5 = \gamma - 1$. The EOS can be simplified as gamma law, which is expressed in (11). According to the gamma law calculation, $\gamma = 1.4$, $C_4 = C_5 = 0.4$, and $E_0 = 2.53 \times 10^6$ J/kg [19, 28].

$$p = C_0 + C_1 + C_2\mu^2 + C_3\mu^3 + \left(C_4 + C_5\mu + C_6\mu^2\right)E_0, \quad (10)$$

with $\mu = (\rho/\rho_0) - 1$,

$$p = (\gamma - 1)\frac{\rho}{\rho_0}E_0, \quad (11)$$

where $p$ is the pressure, $C_0$–$C_6$ are the constants, $\gamma$ represents the rate of change to the specific air temperature, $\mu$ is the dynamic viscosity coefficient, $E_0$ denotes the initial internal energy per unit reference specific volume, $\rho$ represents the current air density, $\rho_0$ is the initial air density value, and $\rho/\rho_0$ denotes the relative density.

## 4. Results and Discussion

*4.1. Validation of Numerical Modelling by the Experimental Results.* The numerical algorithms, material parameters, and numerical models were integrated with experimental data to verify the correctness of the analytical models. This study conducted on-ground explosion experiments to measure the physical quantity of ground acceleration and verify the numerical analysis results, providing numerical models for analyzing the crater. Figures 4 and 5 show the curves for the experimental and numerical ground acceleration for the points 350 and 500 cm from the explosion center. Relative error (%) of peak ground acceleration (PGA) was defined as follows: (numerical analysis value – experimental measurement value)/experimental measurement value × 100%.

The PGAs of the vertical ($Y$) direction for points 350 and 500 cm from the explosion center in the experiment were 1.1932 and 0.9977 m/s$^2$, respectively, and those in the numerical analysis ($Y$) direction were 1.077 and 0.901 m/s$^2$, respectively. The relative errors were −9.71% and −9.73%, respectively, lower than 10%. The PGAs in the horizontal ($X$) direction for points 350 and 500 cm from the explosion center in the experiment were 0.9096 and 0.7371 m/s$^2$, respectively, and the vertical PGAs of the numerical analysis were 0.824 and 0.671 m/s$^2$, respectively. The relative errors were −9.39% and −9.00%, respectively, lower than 10%. The PGAs in the horizontal ($Z$) direction of the experiment were 0.8493 and 0.6118 m/s$^2$, respectively, and the vertical PGAs of numerical analysis were 0.766 and 0.557 m/s$^2$, respectively. The relative errors were −9.84% and −8.96%, respectively. The relative error value is in the range of 10%.

In the experiment of placing the same amount of explosives and measuring waves at 350 and 500 cm from the explosion center, the results showed that high ground acceleration energy was induced near the explosion center. Specifically, the vertical ground acceleration was higher than the horizontal ground acceleration, and the transmission speed in vertical direction declined faster than that in the horizontal direction, which was consistent with the attenuation characteristics of detonation wave energy. The errors of experimental and numerical analysis results were in a reasonable range, which were consistent with related studies [6]. The results also verified that using the MMALE algorithm to establish the numerical model of the fluid-solid interaction could effectively analyze the dynamic characteristics of the explosion phenomenon [17, 20, 21, 28].

The analytical results shown in Figures 4 and 5 reveal a short loading time and high vibration frequency in the dynamic process of the points. Although the ground acceleration yielded by the numerical analysis was not precisely consistent with signals measured in the experiment on-site, the overall dynamic temporal variation curves were consistent with the attenuation characteristics of the shock wave energy. The discrepancy between experimental and numerical analysis results was mainly attributable to the nonuniform, nonlinear dynamic variability in the materials, geometries, conditions, and contact characteristics involved in the shock effect analysis. In addition, the material parameters used in the finite element analysis of instantaneous dynamics must correspond to the dynamic responses obtained from the EOS—namely, changes in the internal energy, temperature, pressure, and volume of the material—and the numerical calculations were affected by the meshed model. According to the analysis results of shock wave transmission in the soil, the temporal variation curves of the ground acceleration produced by the experiment and the numerical analysis were consistent temporally and spatially, and the relative error was within 10%. Therefore, the numerical analysis was satisfactorily effective in estimating the dynamic response of the explosion effects and the material's changes in stress, strain, and volume after receiving external forces.

*4.2. Analysis of Control Parameters for Element Failure.* The LS-DYNA program mainly defines elemental erosion as destruction of material by pressure, stress, and strain parameters and provides settings for material model element failure and the erosion criteria as the basis for evaluating the failed element unit. The simulated material element fails according to the element erosion setting of the MAT_ADD_EROSION model. When element failure and erosion criteria are met, the element is removed from the calculation model. Considering the constitutive law and yield criteria of soil, the material destructive zone is affected by principal strain and shear strain. Therefore, this study examined the parameters of principal strain of failure and shear strain of failure as the main conditions for soil elemental erosion. The crater diameter and depth calculations for the numerical analysis of elemental erosion were based on the position of an eroded element on the axis of symmetry. The relative error percentage (%) of the crater diameter and depth was defined as follows: (numerical analysis value – experimental average value)/experimental average value × 100%.

Figure 6 shows the actual apparent craters of the three explosion experiments. The crater effect caused by the on-ground explosion by placing 226.796 g TNT explosive upright was analyzed. The experimental results indicated that the diameter and depth of the crater of experiment site 1 were 28.00 and 14.89 cm, respectively, experiment site 2 were

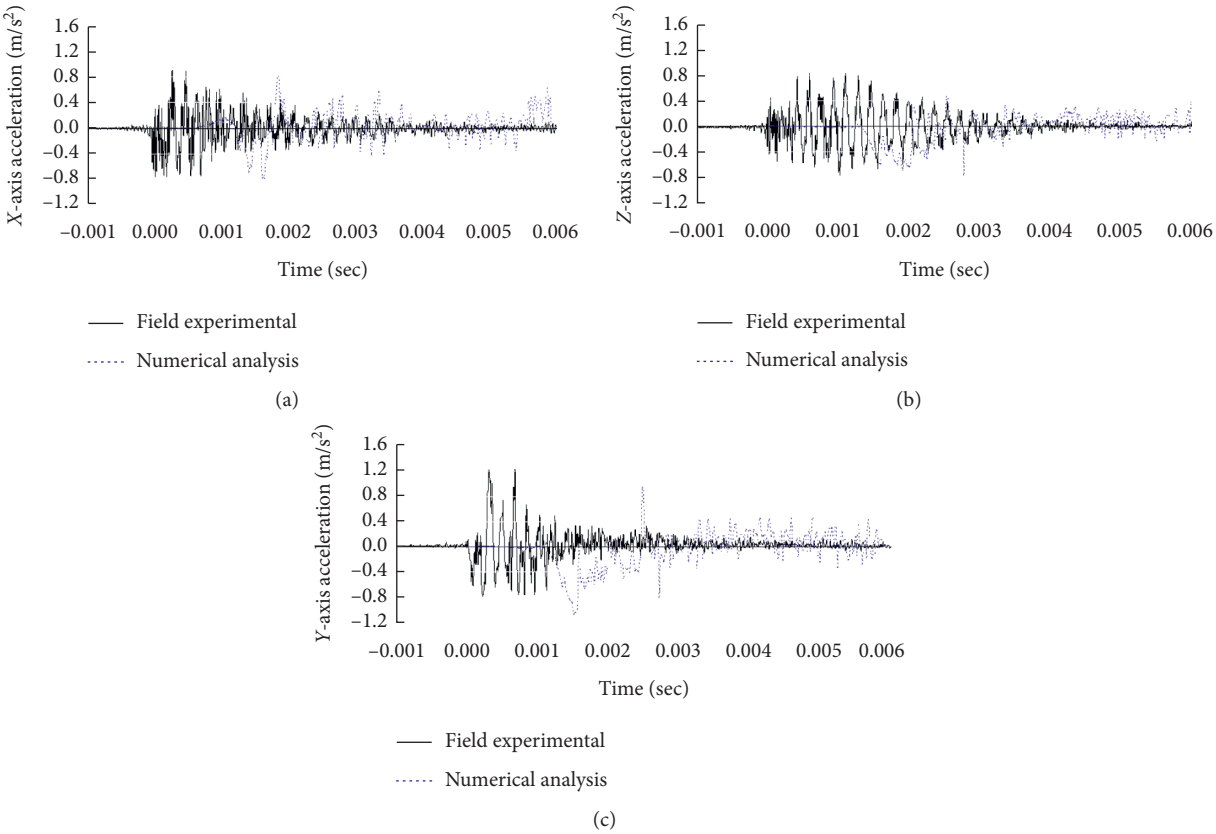


Figure 4: Temporal variation curves of the ground acceleration for a point 350 cm from the explosion center.

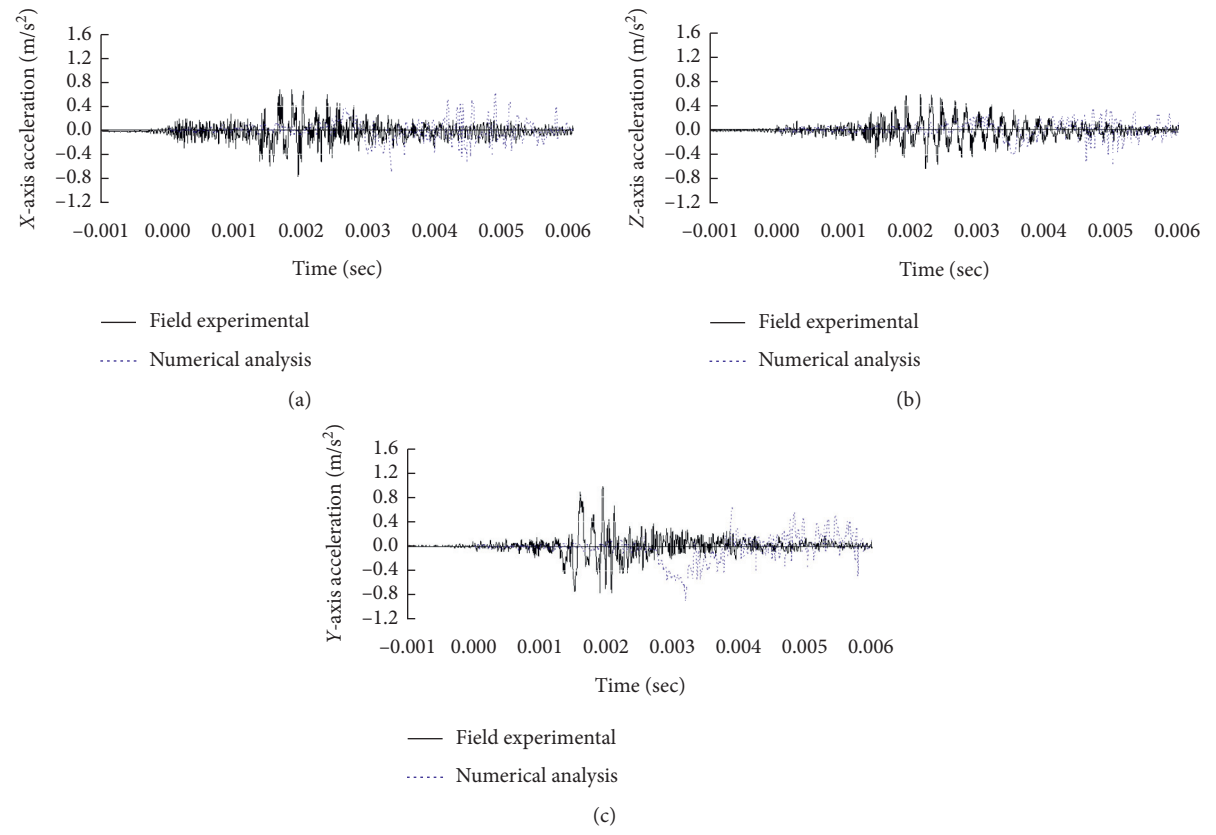


Figure 5: Temporal variation curves of the ground acceleration for a point 500 cm from the explosion center.

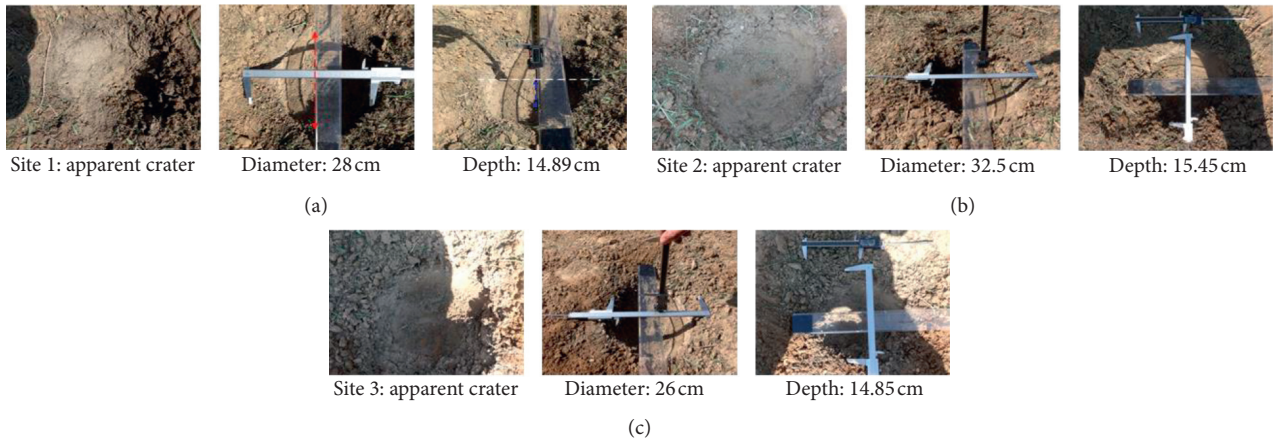


Figure 6: Apparent craters in explosion experiments.

32.50 and 15.45 cm, respectively, and experiment site 3 were 26.00 and 14.85 cm, respectively. The average crater diameter and depth were 28.83 and 15.06 cm, respectively.

Table 1 presents the relative error of principal strain control between the results of numerical simulation and explosion experiment caused by using 226.796 g TNT. The parameter range was between 0.006 and 0.016. The analysis results revealed that the relative error of the crater diameter and depth was −20.36~70.66% and −1.99~63.35%, respectively. The simulation result was most favorable when the failure principal strain value was 0.012. With the increase of the failure principal strain value, crater diameter and element erosion volume became increasingly irregular, mainly due to the material kinematic hardening associated with the high strain rate of explosion.

Table 2 presents a comparison of relative errors between shear strain control of the numerical simulation and experiment caused by using 226.796 g TNT. The analysis results revealed that with the increase in the failure shear strain value, the diameter and depth of the element erosion zone (the crater) decreased. Furthermore, the relative errors of the shear strain control analysis with respect to crater diameter and depth were within the range of −20.36~36.53% and −12.88~52.46%, respectively. Shear strain control resulted in a satisfactory numerical convergence trend. The convergence effect was most favorable when soil failure shear strain was 0.012, and the relative errors between crater diameter and depth were both within 10%.

The results revealed that shear strain and principal strain erosion conditions were the primary control parameters affecting soil element failure. When the failure shear strain value was 0.012, the numerical model exhibited a satisfactory convergence effect. Figure 7 shows the numerical analysis of the explosion caused by 226.796 g TNT. The element erosion condition was set that if the shear strain parameter of the soil reached the critical value of 0.012, the element would be deleted. The results indicated that the relative errors of the experiment were −8.98% and −1.99%, respectively. Using the numerical model established using the shear strain parameters to verify the element erosion algorithm in this study could effectively simulate the element failure of the explosion.

*4.3. Explosion Response and Failure Analysis of Soil.* This study explored the effects of ground explosions on soil deformation and crater effects from the perspective of explosion hazard control. This study conducted on-site explosion experiments and the finite element numerical analysis to analyze the yielding and failure of the protective soil material in the crater effect. This study focused on the destructive effects of high-energy external force, such as instant impact and vibration, caused by contact explosions on the ground medium and the craters created by explosions.

Figure 8 shows the temporal variation of soil plastic strain caused by an explosion of 226.796 g TNT. The figure shows that the detonation pressure was transmitted outward in soil in a spherical shape, and an explosion cavity was formed centering on the explosion source. The energy transmission process was divided into elastic seismic waves and plastic shock waves. The center of the explosion cavity was divided into broken, plastic-elastic, and elastic zones. In addition, the shock wave energy near the explosion center was high, and the compression wave intensity of the soil was relatively high. Figure 9 shows the crater effects caused by on-ground explosions of 113.389 g and 453.592 g TNT samples. For the 113.389 g dynamite sample, the crater diameter was 22.96 cm, and the depth was 13.12 cm. For the 453.592 g TNT sample, the crater diameter was 59.04 cm, and the depth was 22.96 cm.

The analysis results of Figures 7 and 9 show that the shape of the craters was irregular, which was caused by the material displacement, deformation, and failure induced by the shock wave. The primary cause was that the impedance of the shock wave in soil varied with pressure. When the pressure wave reached the free surface and was reflected in the form of a tensile wave, the effects of the expansion wave, pressure wave, and the pressure of the explosive gas caused the tensile wave and shear wave on the ground. The high pressure generated by the nearby explosion resulted in the concentrated and nonuniform distribution that caused local penetrative damage to the elements. Among them, some structural elements increased the dynamic strength because of the rapid rates of strain of the material under dynamic loading.

Table 1: Comparison of principal strain control.

| Failure principal strain | Crater | | | | | |
|---|---|---|---|---|---|---|
| | Diameter | | | Depth | | |
| | Numerical simulation (cm) | Explosion experiment (cm) | Relative error (%) | Numerical simulation (cm) | Explosion experiment (cm) | Relative error (%) |
| 0.006 | 49.20 | 28.83 | 70.66 | 22.96 | 15.06 | 52.46 |
| 0.008 | 49.20 | | 70.66 | 22.96 | | 52.46 |
| 0.010 | 49.20 | | 70.66 | 24.60 | | 63.35 |
| 0.012 | 32.80 | | 13.77 | 16.40 | | 8.90 |
| 0.014 | 32.80 | | 13.77 | 16.40 | | 8.90 |
| 0.016 | 22.96 | | −20.36 | 14.76 | | −1.99 |

Table 2: Comparison of relative errors for shear strain control.

| Failure shear strain | Crater | | | | | |
|---|---|---|---|---|---|---|
| | Diameter | | | Depth | | |
| | Numerical simulation (cm) | Explosion experiment (cm) | Relative error (%) | Numerical simulation (cm) | Explosion experiment (cm) | Relative error (%) |
| 0.006 | 39.36 | 28.83 | 36.53 | 22.96 | 15.06 | 52.46 |
| 0.008 | 32.80 | | 13.77 | 21.32 | | 41.57 |
| 0.010 | 32.80 | | 13.77 | 16.40 | | 8.89 |
| 0.012 | 26.24 | | −8.98 | 14.76 | | −1.99 |
| 0.014 | 26.24 | | −8.98 | 14.76 | | −1.99 |
| 0.016 | 22.96 | | −20.36 | 13.12 | | −12.88 |

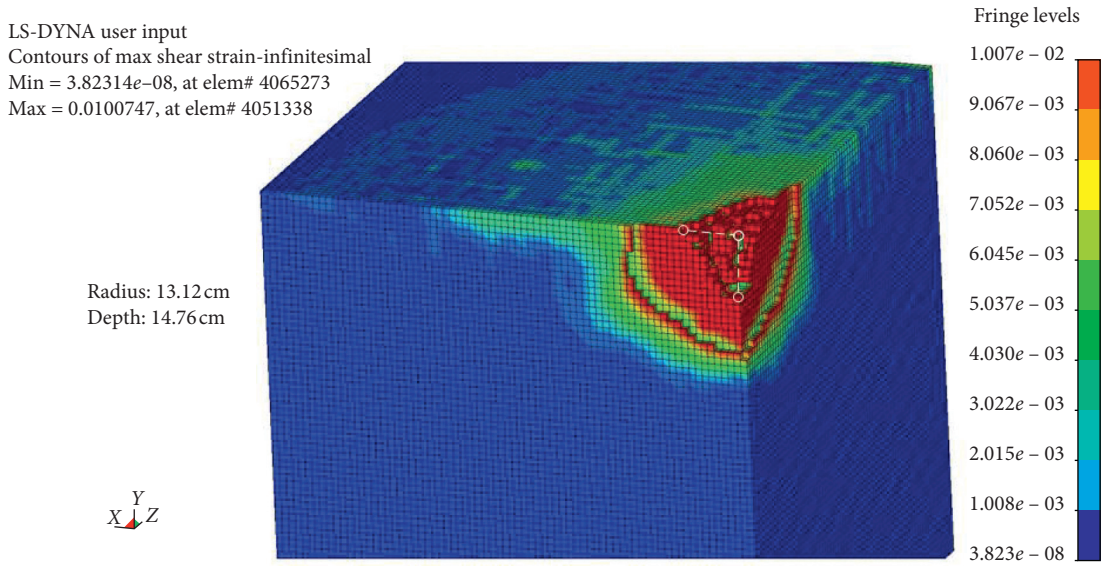


Figure 7: Numerical analysis of the element erosion of the crater caused by the on-ground explosion by using a 226.796 g (0.5 lb) TNT.

The results indicated that if the amount of the explosive was increased multiple times, the radius and depth of the crater would increase, and the radius of the failure area would also increase multiple times. The radius of the crater was approximately 10~12 times the width of the rectangular dynamite samples, and the depth of the plastic zone was approximately 1.8~2.2 times the radius of the crater; the area was the affected range of the plastic shock wave. The energy outside the region was converted into elastic seismic waves, which induced surface particle vibration.

In addition, soil was a low-tensile material. Under the impact of the explosion shock wave, the acceleration of the particle motion increased the shear stress in the soil body. The soil structure was subjected to stress concentration because of the uneven distribution of stress, resulting in a decrease in shear strength. The compression wave caused particle displacement, and the failure started from local plastic deformation. The analysis results showed that under the effect of shock wave, the shear stress failure zone would appear in the periphery of the crater. The primary feature

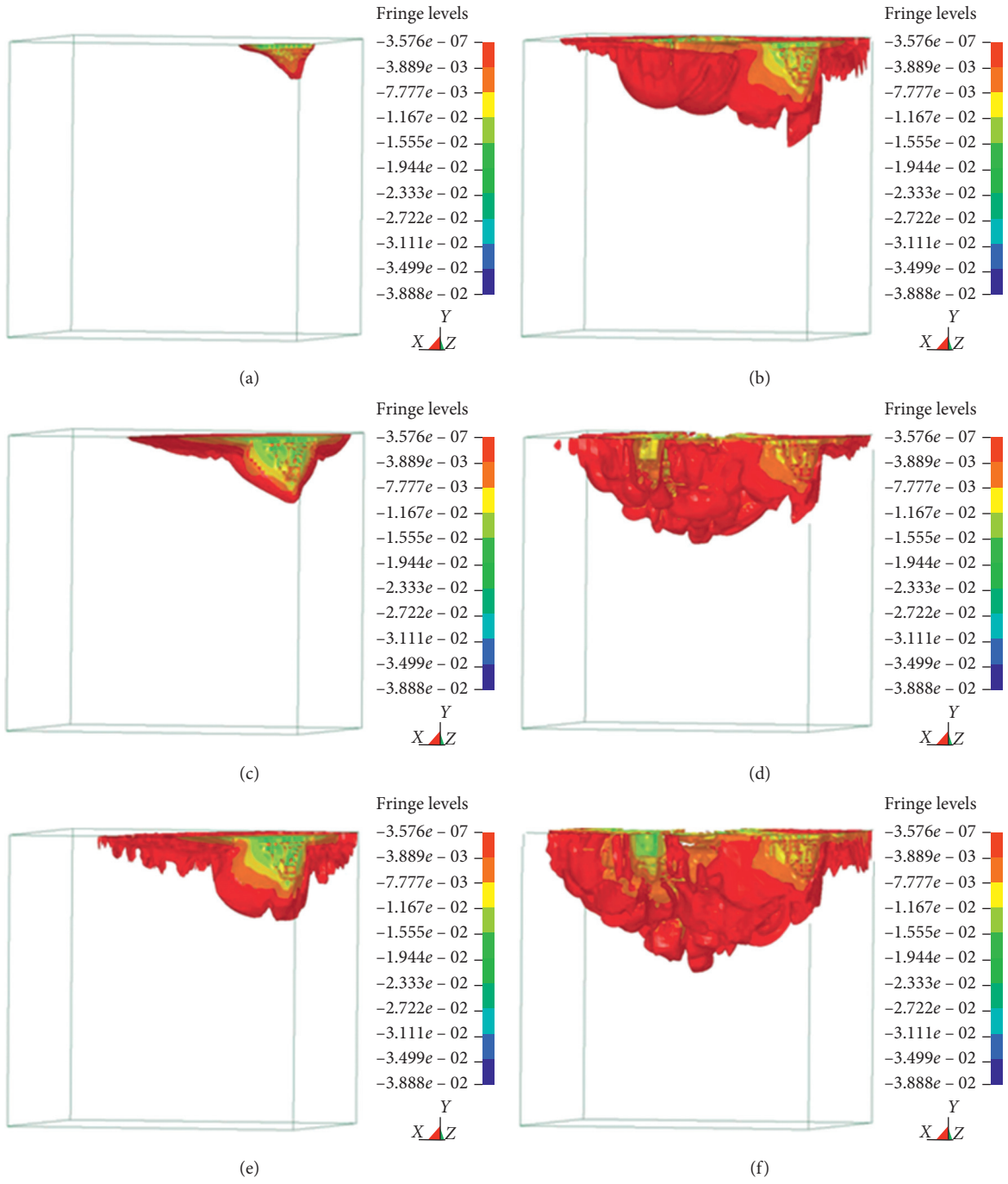


Figure 8: Temporal variation of soil plastic strain induced by an explosion. (a) $t = 99.89\,\mu s$. (b) $t = 1{,}499.90\,\mu s$. (c) $t = 499.88\,\mu s$. (d) $t = 2{,}000.00\,\mu s$. (e) $t = 999.84\,\mu s$. (f) $t = 2{,}499.90\,\mu s$.

was that the soil medium was plastically deformed. As the stress wave passed, if the second invariant ($J_2$) of the stress deviation of the particle was higher than the yield strength of the material, plastic shearing would be generated in the region, resulting in permanent deformation and destruction.

Based on the aforementioned results, the sudden change in pressure caused by the explosion resulted in substantial deformation and destruction of the material. Shock wave was a strong compression wave. The shock wave generated by explosions was transmitted in the soil medium. The energy was mostly depleted by the deformation, destruction, and pushing of the surrounding medium. Soil was a three-phase material composed of solid, liquid, and gas. The plasticity of soil was high, the strength was low, and compressive strength was higher than the tensile and shear strength. In addition, the explosion effect changed the stress state of the material, and if the stress exceeded the material yield strength, the internal structural stability would be affected, leading to soil deformation, local failure, and the affected range of stress.

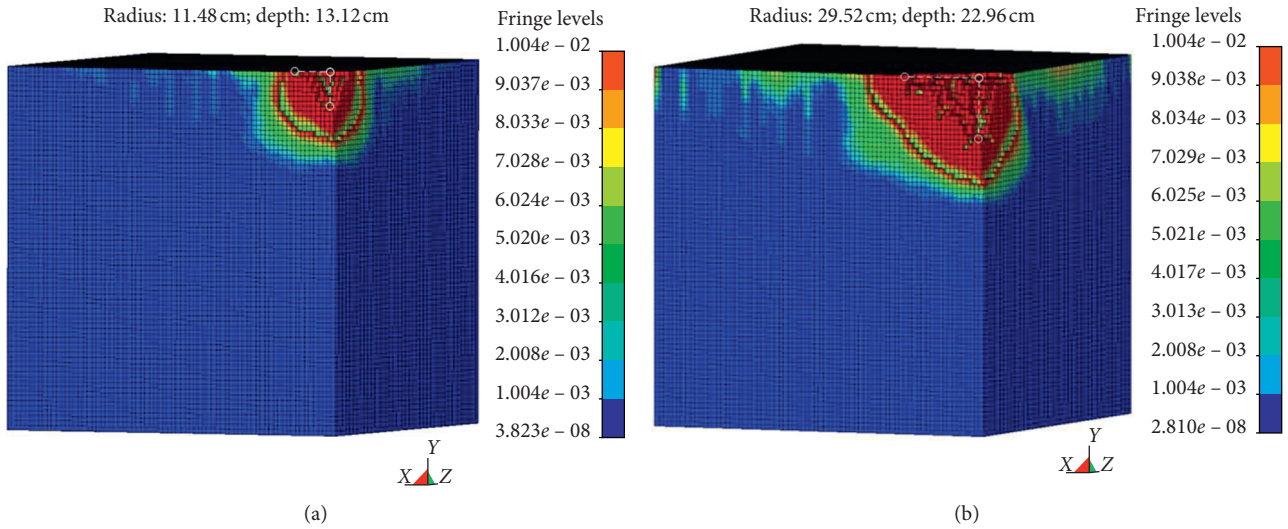


Figure 9: Numerical analysis of element erosion of the crater created by (a) 0.25 lb TNT (113.389 g) and (b) 1.0 lb TNT (453.592 g).

The explosion caused points on the ground surface to vibrate. The dynamic material response analysis was conducted according to the pressure applied to, stress of, and strain of the material. Shock waves were transmitted through mediums. A high strain rate changed the stress state of the material; when the stress exceeded the material's yield strength, plastic deformation occurred, and displacement increased, which in turn undermined the material stability. The transmission of shock waves was affected by the material properties of the transmission medium and terrain at the experimental site. From the perspective of controlling shock effects and minimizing damage, this study estimated the intensity and spatial range of damage caused by shock waves through the analysis of material deformation, temporal variation of plastic strain, displacement, and shear strain. The results could be conducive to determining the soil-covering layer material and the protective soil layer thickness to produce effective strength, thus preventing the transmission of shock wave energy. Additionally, the analysis of the ground surface vibration effect and a vibration isolation design could effectively block the transmission of shock waves, in turn reducing vibrations and minimizing the damage.

## 5. Conclusions

This study analyzed the failure characteristics of transmission medium caused by the shock wave. By using explosion-induced ground acceleration, this study verified the numerical model to establish an effective numerical analysis model for explosion. The hazards caused by craters created by explosions were explored. The material failure criterion and the finite element erosion algorithm were used to analyze the plastic deformation and destruction area of the soil. The results of this study can serve as a reference for the control of explosion vibration hazards, explosion at the exterior of protective soil, and disaster prevention. The results of the study are summarized as follows:

(1) The numerical analysis of this study used an 8-node hexahedral element to establish a solid structural model of the fluid-solid interaction using the MMALE algorithm. A 3D numerical model was established by combining the shear strain parameters of the element erosion algorithm to analyze the crater effect of the explosion. The experimental results showed that the numerical model could effectively analyze the dynamic response of nonlinear materials, the hydrodynamic behavior generated by explosions, and the temporal pressure change of explosions.

(2) A typical explosion is characterized by a sudden change in pressure at the explosion site. For the destruction phenomena in this study, the transmission of high-intensity shock waves affected material stability. The soil was affected by uneven stress, and the failure conditions of the material were affected by the stress and shear strain. The transmission of shock wave in soil was primarily caused by the increase of the inertial force that led to the decrease in shear strength; and the secondary cause was the continuous vibration effect that induced the increase in shear stress of the soil body and affected the stability of the material.

(3) The stress state of the material that has been affected by explosive vibration changes tends to influence the structure and strength of the soil body. In this study, during the shock wave transmission process, the essential condition of failure was the plastic deformation and shear strain increment caused by the exceeded material yield strength. The ground surface was strongly compressed, destroying its original material structure. The soil was compressed by shock waves and crater was formed. The plasticity of the soil body varied with the pressure of shock wave and the extent of destruction varied. The area encompassing the crater radius and the depth of 1.8~2.2

times the crater radius was the plastic concentration zone of shear failure. In this region, the material was affected by compression, crushing, deformation, and destruction.

## Data Availability

The data used to support the findings of this study are available from the corresponding author upon request.

## Conflicts of Interest

The author declares that there are no conflicts of interest.

## Acknowledgments

The author thanks the engineering advisory group of the Ministry of National Defense in Southern Taiwan R.O.C. for assisting in this study.

## References

[1] I. T. Wang, "Field experiments and numerical analysis of the ground vibration isolation of shock wave propagation under explosion shock loading," *Vibrations*, vol. 2, no. 4, pp. 300–310, 2019.

[2] K. Balakrishnan, F. Genin, D. V. Nance, and S. Menon, "Numerical study of blast characteristics from detonation of homogeneous explosives," *Shock Waves*, vol. 20, no. 2, pp. 147–162, 2010.

[3] E. Wang and A. Shukla, "Analytical and experimental evaluation of energies during shock wave loading," *International Journal of Impact Engineering*, vol. 37, no. 12, pp. 1188–1196, 2010.

[4] S. E. Rigby, S. D. Fay, A. Tyas et al., "Influence of particle size distribution on the blast pressure profile from explosives buried in saturated soils," *Shock Waves*, vol. 28, no. 3, pp. 613–626, 2017.

[5] L. B. Jayasinghe, D. P. Thambiratnam, N. Perera, and J. H. A. R. Jayasooriya, "Blast response and failure analysis of pile foundations subjected to surface explosion," *Engineering Failure Analysis*, vol. 39, pp. 41–54, 2014.

[6] A. Schenker, I. Anteby, E. Gal et al., "Full-scale field tests of concrete slabs subjected to blast loads," *International Journal of Impact Engineering*, vol. 35, no. 3, pp. 184–198, 2008.

[7] Z. Wang and Y. Lu, "Numerical analysis on dynamic deformation mechanism of soils under blast loading," *Soil Dynamics and Earthquake Engineering*, vol. 23, no. 8, pp. 705–714, 2003.

[8] F. J. Crandle, "Ground vibration due to blasting and its effect upon structures," *Journal of Boston Society of Civil Engineers*, vol. 36, pp. 222–245, 1949.

[9] Y. Koga and O. Matsuo, "Shaking table tests of embankments resting on liquefiable sandy ground," *Soils and Foundations*, vol. 30, no. 4, pp. 162–174, 1990.

[10] Z. Wang, H. Hao, and Y. Lu, "A three-phase soil model for simulating stress wave propagation due to blast loading," *International Journal for Numerical and Analytical Methods in Geomechanics*, vol. 28, no. 1, pp. 33–56, 2004.

[11] J. Wang, "Simulation of landmine explosion using LS-DYNA 3D software: benchmark work of simulation in soil and air," pp. 1–30, DSTO Aeronautical and Maritime Research Laboratory, Fishermans Bend, Australia, 2001, DSTO-TR-1168.

[12] J. M. Duncan and C.-Y. Chang, "Nonlinear analysis of stress and strain in soils," *Journal of the Soil Mechanics and Foundations Division*, vol. 96, no. 5, pp. 1629–1653, 1970.

[13] G. W. Ma, H. Hao, and Y. X. Zhou, "Modeling of wave propagation induced by underground explosion," *Computers and Geotechnics*, vol. 22, no. 3-4, pp. 283–303, 1998.

[14] R. D. Ambrosini and B. M. Luccioni, "Craters produced by explosions on the soil surface," *Journal of Applied Mechanics*, vol. 73, no. 6, pp. 890–900, 2005.

[15] Z. P. Bazant and T. B. Belytschko, "Wave propagation in a strain softening bar-exact solution," ASCE," *Journal of Engineering Mechanics*, vol. 3, pp. 381–389, 1985.

[16] R. W. Clough and R. J. Woodward, "Analysis of embankment stresses and deformations," *Journal of the Soil Mechanics and Foundations Division*, vol. 93, no. 4, pp. 529–549, 1967.

[17] C. Wu and H. Hao, "Modeling of simultaneous ground shock and airblast pressure on nearby structures from surface explosions," *International Journal of Impact Engineering*, vol. 31, no. 6, pp. 699–717, 2005.

[18] LS-DYNA, *Theoretical Manual*, pp. 1–117, Livermore Software Technology Corporation, Finite Element Model Builder, Livermore, CA, USA, 2006.

[19] LS-DYNA, *Keyword User's Manual*, vol. 1, pp. 37–2435, Livermore Software Technology Corporation, Livermore, CA, USA, 2010.

[20] M. S. Chafi, G. Karami, and M. Ziejewski, "Numerical analysis of blast-induced wave propagation using FSI and ALE multi-material formulations," *International Journal of Impact Engineering*, vol. 36, no. 10, pp. 1269–1275, 2009.

[21] Y.-T. Wang and J.-Z. Zhang, "An improved ALE and CBS-based finite element algorithm for analyzing flows around forced oscillating bodies," *Finite Elements in Analysis and Design*, vol. 47, no. 9, pp. 1058–1065, 2011.

[22] M. A. Puso, J. Sanders, R. Settgast, and B. Liu, "An embedded mesh method in a multiple material ALE," *Computer Methods in Applied Mechanics and Engineering*, vol. 245-246, pp. 273–289, 2012.

[23] L. Schwer, *Geomaterial Modeling with LS-DYNAU*, pp. 1-2, Livermore Software Technology Corporation, Livermore, CA, USA, 2001.

[24] N. Gebbeken and M. Ruppert, "On the safety and reliability of high dynamic hydrocode simulations," *International Journal for Numerical Methods in Engineering*, vol. 46, no. 6, pp. 839–851, 1999.

[25] I. T. Wang, "Numerical and experimental verification of finite element mesh convergence under explosion loading," *Journal of Vibroengineering*, vol. 16, no. 4, pp. 1786–1798, 2014.

[26] B. M. Dobratz and P. C. Crawford, *LLNL Explosives Handbook: Properties of Chemical Explosives and Explosive Simulants*, Report UCRL-52997, pp. 208–230, Lawrence Livermore National Laboratory, Livermore, CA, USA, 1985.

[27] A. Erdik, S. A. Kilic, N. Kilic, and S. Bedir, "Numerical simulation of armored vehicles subjected to undercarriage landmine blasts," *Shock Waves*, vol. 26, no. 4, pp. 449–464, 2016.

[28] Y. S. Tai, T. L. Chu, H. T. Hu, and J. Y. Wu, "Dynamic response of a reinforced concrete slab subjected to air blast load," *Theoretical and Applied Fracture Mechanics*, vol. 56, no. 3, pp. 140–147, 2011.